IEEE Access
Multidisciplinary | Rapid Review | Open Access Journal

Received April 1, 2019, accepted April 17, 2019, date of publication April 29, 2019, date of current version May 14, 2019.

Digital Object Identifier 10.1109/ACCESS.2019.2913692

Noise Modeling in Field Emission and Evaluation of the Nano-Receiver in Terms of Temperature

KEITA FUNAYAMA[1,2], HIROYA TANAKA[1], (Senior Member, IEEE), JUN HIROTANI[2], KEIICHI SHIMAOKA[1], YUTAKA OHNO[2,3], AND YUKIHIRO TADOKORO[1], (Senior Member, IEEE)

[1]Toyota Central Research and Development Laboratories, Inc., Nagakute 480-1192, Japan
[2]Department of Electronics, Nagoya University, Nagoya 464-8603, Japan
[3]Institute of Materials and Systems for Sustainability, Nagoya University, Nagoya 464-8603, Japan

Corresponding author: Keita Funayama (funayama@mosk.tytlabs.co.jp)

This work was supported by the Nagoya University Microstructural Characterization Platform as a "Nanotechnology Platform" Program, Ministry of Education, Culture, Sports, Science and Technology (MEXT), Japan.

ABSTRACT The field-emission phenomenon is exploited in a broad variety of applications and systems. Previous studies have reported that the current induced by field emission strongly and inherently depend on the temperature. This dependence enhances the noise in the current, which results in performance degradation in, for example, signal detection and communications in nanoscale receivers. In this paper, a mathematical model is presented for the suppression of the noise based on its probability density. Our experiment and analysis revealed that the density follows a Gaussian distribution, and the dependence on temperature is observed to be exponential. This result is intriguing because in the field of signal processing and communication, the influence of temperature is often considered with a noise-temperature model, namely, linear dependence. Using our derived model, we theoretically evaluated the communication performance of a nanoscale receiver; owing to the exponential dependence on temperature, severe performance degradation was found with increasing temperature. This means that, as field-emission technology continues to be developed, the temperature should be kept low, for example, at room temperature, to secure the reliability of nanoscale communication devices.

INDEX TERMS Bit-error rate, field emission, nanoscale communication, nonlinear temperature dependence.

I. INTRODUCTION

The extensive application of the field-emission phenomenon has been reported in various fields [1]–[9]. Owing to its interesting characteristic that induces a current in microscopic systems, atomic-level objects can be observed [3], [4], and the downsizing of displays is possible [5], [6]. In recently developed nanomechanical systems, current measurement enables estimation of the amplitude of a vibration in nano-meters. Many researchers are paying attention to this type of the system because it has the potential to create a paradigm shift in various fields, such as signal processing [10]–[14], communications [15]–[24], and sensing applications [25]–[30]. Despite these attractive features, the noise in the current makes the system stochastic, which degrades performance.

Field emissions are inherently affected by the variation in temperature. In the past several decades, the general theory has been discussed in the literatures, e.g., [31], [32], and experimental demonstrations have been provided for various types of emitters, including thermally grown SiO_2 emitters [33], carbon-based emitters [34]–[37], and $W_{18}O_{49}$ nanowires [38]. As the temperature increases, the obtained current is enhanced. This is because the work function on the emitter depends on the temperature; from Fowler–Nordheim theory, which is briefly described in Section II, the current strongly depends on the work function. This result is supported by the experiments using, for example, $SiC@SiO_2@$graphene nanoarray emitters [35] and VO_2(A) nanogap emitter [39]. It is also observed that the fluctuation in the current, namely, the noise component, also increases with the increase in temperature [35], [37].

To capture the behavior of noisy systems, a noise model based on a probability density is beneficial. The time evolution of the system behavior in, for example, nanomechanical systems and biological systems, is described by a stochastic differential equation for the probability density. In the field

The associate editor coordinating the review of this manuscript and approving it for publication was Emrecan Demirors.

of signal processing, the error rates of signal detection are analytically evaluated with a probability density [40], [41]; a typical example is the nanoscale receiver, whose performance has been demonstrated to strongly depend on the probability density of the noise [18]. Against the importance of the probability density, for semiconductor devices, fluctuation or noise is usually evaluated in the frequency domain; field emission on carbon-based materials such as carbon nanotube (CNT) and graphene has been investigated, and the noise in the resulting current has been reported to have an inverse frequency dependence [34], [42]–[44]. This behavior is found in other types of the emitters, including WS_2 nanosheets emitter [34]. The probability density of the noise should be investigated to aid the development of a variety of applications and systems with this current. The dependence on temperature should be considered in the investigation.

In this study, for the future development of a wide variety applications and systems based on field emissions, we attempt to build a concrete model of noise dependence on temperature. By measuring the noise in the current and performing nonparametric modeling with kernel density estimation (KDE), we showed that the probability density of the noise follows a Gaussian distribution. An accurate fitting to the proposed model indicated that the dependence on temperature is exponential; this is an interesting result because the influence of temperature is often considered with a noise-temperature model that incorporates linear dependence. Our analysis also showed that the impact of noise on the communication performance of the nanoscale receiver increases greatly as the temperature increases. We focused on the error rate in the reception of digital data, namely, the bit-error rate (BER), which exponentially increases with temperature.

This paper is organized as follows. A brief review of field emissions is provided in Section II. Based on our measurement results, the analytical model of the probability density is derived in Section III. The model is revealed to be Gaussian in Section III-A, and the two key parameters, mean and variance, are analytically described as a function of the temperature in Section III-B. By focusing on a nanoscale receiver [18], we analytically discuss the influence of the temperature on performance in Section IV. Concluding remarks are given in Section V.

II. BRIEF REVIEW OF FIELD-EMISSION THEORY

The phenomenon of field emission has long been investigated in semiconductor physics and devices [31], [33], [42], [44]–[47]. When a sufficiently high voltage is applied between two electrodes, one of which has a sharp shape and is separated from the other by a small gap, the strongly induced electric field promotes the emission of electrons from the sharp material. The resulting field-emission current is theoretically characterized by the well-known Fowler–Nordheim equation: for the electronic field between the electrodes $E(V)$, which is induced by the applied voltage V, the current is modeled as [31]–[33]

$$I(V) = \frac{C_1 E(V)^2}{t^2(y)} \exp\left(-\frac{C_2 v(y)}{E(V)}\right), \tag{1}$$

where

$$t(y) \equiv \{(1+y)H[\kappa] - yK[\kappa]\}/\sqrt{1+y} \tag{2}$$

$$v(y) \equiv \{H[\kappa] - yK[\kappa]\}\sqrt{1+y} \tag{3}$$

are the correction terms with $\kappa \equiv \sqrt{(1-y)/(1+y)}$ and $y \equiv \sqrt{eE(V)/4\pi\epsilon_0}/W_{\rm f}$. If we define $W_{\rm f}$ as the work function of the emitter and $S \equiv \pi\rho^2$ as the area that emits electrons, then $C_1 \equiv e^2 S/8\pi h W_{\rm f}$ and $C_2 \equiv 8\pi(2\,em_{\rm c})^{\frac{1}{2}} W_{\rm f}^{\frac{3}{2}}/3h$. h is the Planck constant, e is the elementary charge, $m_{\rm c}$ is the mass of the electron, ϵ_0 is the permittivity of free space, and $K[\cdot]$ and $H[\cdot]$ are the complete elliptic integrals of the first and second kind, respectively. If the emitter is the tip of a carbon nanotube (CNT), the electric field is given as $E_z(V) = \beta V/z$ where z is the length of the gap between the CNT tip and electrode, $\beta \equiv L/2\rho$ is the enhancement factor [45], and ρ and L are the radius and length of the CNT, respectively.

The Fowler–Nordheim equation (1) is provided when the temperature T is approximately 0 K. Since their pioneering work [46], the dependence of the current on the temperature has been investigated. The influence of temperature can be considered by multiplying by a temperature-dependent term,

$$\vartheta(T) \equiv \frac{\frac{C_3 T}{E_z(V)}}{\sin\left(\frac{C_3 T}{E_z(V)}\right)}, \tag{4}$$

where $C_3 \equiv (4\pi^2\, k_{\rm B} t(y)/h)\sqrt{2\, m_{\rm c} W_{\rm f}/e}$ with the Boltzmann constant $k_{\rm B}$ [32], [33], [48]. The current is, therefore, given as

$$I_z(V;T) = I(V)\vartheta(T). \tag{5}$$

The noise in the current has been measured in various emitters [34], [42]–[44], and discussed in the frequency domain. Against these meaningful investigations, we reveal the probability density of the noise in this work.

To measure the field-emission current, we created a singly clamped multi-wall CNT (MWCNT) emitter, which was fabricated on silicon wafer as shown in Fig. 1(a). The MWCNTs were produced by an arc discharge process to secure straight MWCNTs. Such MWCNTs, which were contained in a solvent, were dropped on a silicon wafer, which had a 3μm-thick silicon dioxide layer. The solvent was quickly evaporated by heating. For the MWCNTs with length and radius of $L = 1.1\,\mu$ m and $\rho = 6.72$ nm, respectively, a cathode was directly deposited on an edge of the MWCNT. The anode was also deposited away from the tip of a MWCNT emitter at a distance of approximately 105 nm. The electrodes were fabricated by electron-beam lithography and metal evaporation. They consisted of 10 nm Ti and 100 nm Au. The silicon dioxide under a MWCNT was etched by buffered hydrofluoric acid to realize the MWCNT cantilever.

For the above device, the current was measured with a semiconductor device analyzer (Keysight B1500A). A voltage was applied between the anode and cathode via the

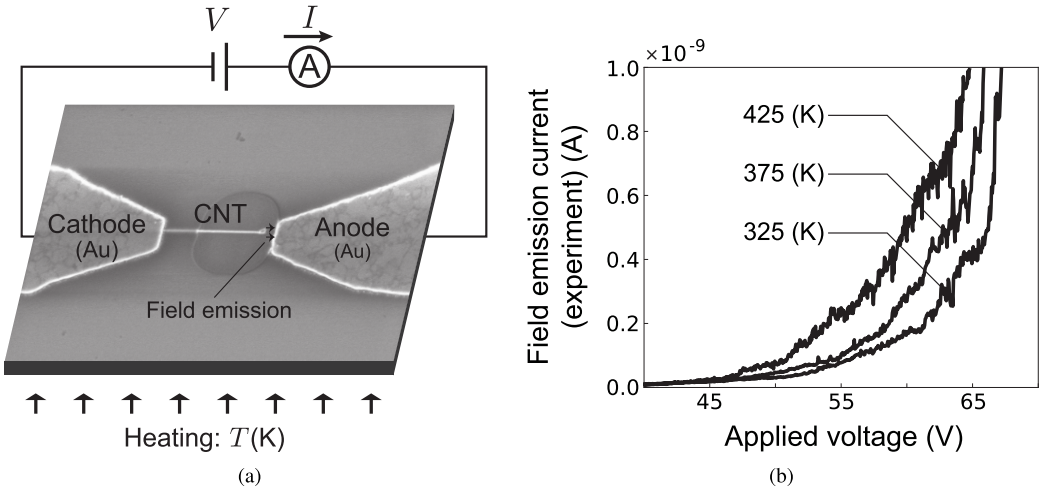

FIGURE 1. (a) System diagram for testing field emissions. In the scanning electron microscope image of our fabricated device, the emitter is a multi-wall CNT with length $L = 1.1\,\mu$m and radius $\rho = 6.72$ nm. The emitting part, that is, the tip of the CNT, is separated from the counter electrode by $z = 105$ nm. To vary the temperature, the sample with the CNT and electrode is placed on a heating device. (b) Measured tunnel current. The observed exponential behavior is evidence of the field emission current. Temperature dependence, which is predicted in (5), is also found.

analyzer, and the field emission current was measured in a vacuum (8.2×10^{-3} Pa). The MWCNT emitter was placed on a heating plate to change the temperature, as shown in Fig. 1(a). The temperature was set via a controlling device, Scientific Instruments 9700. As shown in Fig. 1(b), a distinct exponential increase is observed; this is evidence of the field emission. We also see the temperature dependence predicted by (5).

As described in [33], fitting experimental data to the analytical model in (5) requires consideration of the dependence of the work function on the temperature. This is achieved by introducing a fitting parameter, $a(T)$, such that the correction term $v(y)$ depends on the temperature. The value of the two parameters can be obtained by minimizing the error between the experimental data and the theoretical value obtained by (5).

III. MODELING THE PROBABILITY DENSITY OF THE TUNNEL CURRENT IN TERMS OF TEMPERATURE

In this section, the measured current is used to derive the analytical expression of the probability density. In Section III-A, the probability density of the measured current is found to have a Gaussian distribution. The analytical expression of the two key distribution parameters, mean and variance, are presented in Section III-B.

A. MODELING THE SHAPE OF THE PROBABILITY DENSITY

The current was measured 10 times for each of three given temperatures. In the measurement, first, we determine the applied voltage, which is used in the measurement for the temperature dependence. The voltage was swept, as shown in Fig. 1(b), and determined to be 65 V to prevent overcurrent of the emitter. For each temperature, the current was measured 10 times; in each single measurement, the current was measured for 5 s. After the single measurement, the voltage was not applied for a sufficient time interval (60 s) to initialize the measurement. For the data collected at each temperature, the three data with the largest slopes were discarded to avoid the time drift.

The left panels in Fig. 2 show examples of the measured current at $T = \{325, 375, 425\}$ K. Although the current slightly increases along with increasing temperature, the amplitudes of the currents fluctuate over time. This behavior is the noise in the current, and the purpose of this work is to derive a theoretical model for this fluctuation.

Noise is often characterized by a probability density. For example, it is well-known that the amplitude of thermal noise follows a Gaussian probability density. To derive the theoretical model of this fluctuation, first, we capture the trend of the density with KDE, a non-parametric method [49]–[51]. When N sample points of current I_i $(1 \le i \le N)$ are obtained in a single measurement, the corresponding probability density of the current, $\Pr[I]$, is given by the sum of the kernel function $g(x)$:

$$\Pr[I] = \frac{1}{N}\sum_{i=1}^{N} g\left(\frac{I - I_i}{W}\right), \tag{6}$$

where W is the bandwidth. Note that in this analysis, the noise is treated as white; in many devices, the noise is filtered out, especially outside the focused frequency-band. The residual noise has a small bandwidth, which indicates that the noise can be treated as white.

The measured densities (6) are plotted with dots in the center panels of Fig. 2. Three temperatures, 325 K, 375 K, and 425 K, were used, and $N = 70$. The Gaussian kernel with zero mean and unit variance, $g(x) = (1/\sqrt{2\pi})\exp(-x^2/2)$, was used. The parameter W was determined by a widely used method, Scott's rule [50], [52]. In all cases, the curve of the

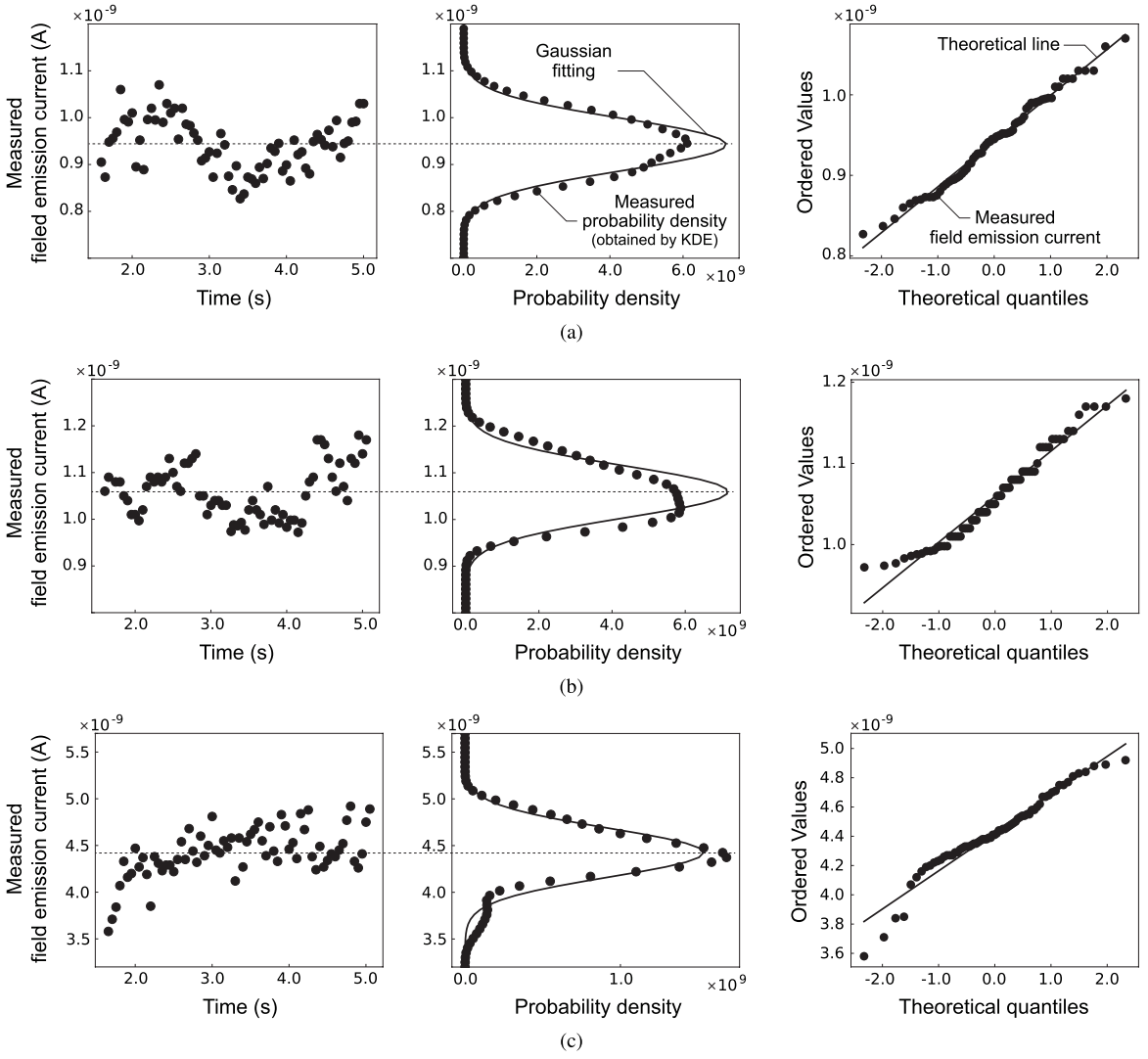

FIGURE 2. Measured examples of the field-emission current and the corresponding probability densities at (a) $T = 325$ K, (b) $T = 375$ K, and (c) $T = 425$ K. The measured currents are plotted in the left panels, and the corresponding probability densities calculated with (6) are presented by solid circles in the center panels. The densities are found to follow a Gaussian distribution which is depicted with solid curves fitted to the points with the measured average $\hat{\mu}$ and variance $\hat{\sigma}^2$. This observation is confirmed in the normal Q-Q plots provided in the right panels; the measured points are located along the theoretical line, and the degree of the determination is (a) 0.99487, (b) 0.98247, and (c) 0.97543.

density has one peak and does not have a heavy tail. Intuitively, these densities should follow a Gaussian distribution.

The above Gaussian model is confirmed by observing the theoretical curves of the Gaussian distributions with the measured average $\hat{\mu} \equiv \frac{1}{N}\sum_i I_i$ and variance $\hat{\sigma}^2 \equiv \frac{1}{N}\sum_i I_i^2 - (\frac{1}{N}\sum_i I_i)^2$. These curves are plotted with solid lines in the center panels of Fig. 2, which show that the distributions agree with the measured densities. To evaluate the distributions more clearly, normal quantile-quantile (Q-Q) plot are provided in the right panels. Almost all of the measured sample points are located along the theoretical line and the degree of determination is greater than 0.97. These observations are also found in the other measurements. Therefore, it can be stated that the probability density of the current follows a Gaussian distribution. The theoretical model of the current is given by

$$\Pr[I] = \frac{1}{\sqrt{2\pi\sigma^2}}\, exp\left[-\frac{(I-\mu(T))^2}{2\sigma^2(T)}\right], \tag{7}$$

where $\mu(T)$ is the mean and $\sigma^2(T)$ is the variance.

B. MODELING OF THE MEAN AND VARIANCE

The next task is modeling the key parameters in the distribution, μ and σ^2. If the current follows a Gaussian distribution, the most expected amplitude is the mean. This amplitude is often measured in many studies, and it has been modeled by the well-known expression (5). In this sense, the mean can be modeled as

$$\mu(T) = I\ (V;\ T) = I(V)\ \vartheta\ (T). \tag{8}$$

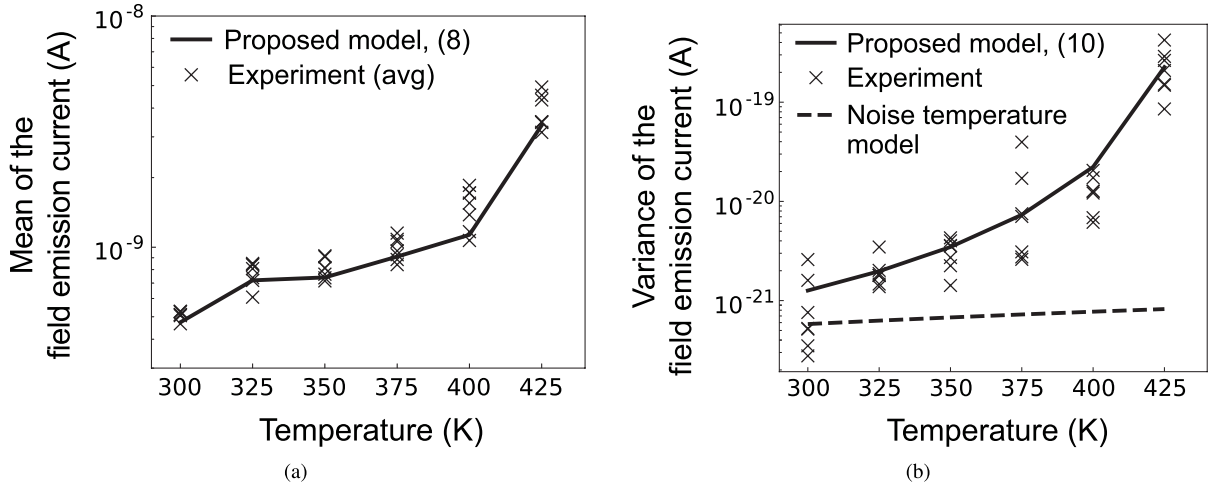

FIGURE 3. Numerical examples of the analytical model for (a) mean (8) and (b) variance (10) are presented with solid curves. The measured average $\hat{\mu}$ and variance $\hat{\sigma}^2$ are also marked as ×'s. The analytical model accurately describes the mean and variance as they change according to temperature because the analytical curves are located within the range of the measured data points. The theoretical curve of the noise temperature model, which is often used to consider the influence of the temperature, is also plotted with a dotted line in (b). Clearly, the slope in the noise temperature model is quite different from that of the field-emission current, which indicates that our developed model is beneficial to model the noise in field-emission current.

With the asymptotic notations, the mean is rewritten as $\mu(T) = O_T(\vartheta(T))$, where the subscript T in O notation indicates that the order is considered in terms of the temperature T.

The variance is analytically modeled from (5). Because variance is a second-order statistic, the variance term $\sigma^2(T)$ is the squared order of the current. Thus,

$$\sigma^2(T) = O_T\left(I^2(V;T)\right) = O_T\left(\vartheta^2(T)\right). \tag{9}$$

This expression indicates that the variance can be modeled by the order of $\vartheta^2(T)$. Introducing the two parameters A and B gives us the form,

$$\sigma^2(T) = A\left(\frac{BT}{\sin BT}\right)^2. \tag{10}$$

The values of A and B can be obtained by fitting to the measured current.

The analytical models of the mean and variance, (8) and (10), respectively, are evaluated with the measured current. To calculate the average, $W_\mathrm{f} = 4.8\,\mathrm{eV}$ for CNT was used [53]. The field intensity included in (8) was multiplied by the constant b to consider the influence of the finite size of the anode. Numerical fitting yielded $A = 2.08\times10^{-22}$ and $B = 2.30\times10^{-3}$. Figure 3 shows that the measured $\hat{\mu}$ and $\hat{\sigma}^2$, which are plotted as ×'s, exponentially increase with increasing temperature. In fact, the mean at $T = 325\,\mathrm{K}$ seems to not follow exponential behavior; in the numerical fitting process, the parameter $a(T)$ at this temperature results in a large variation due to a measurement error. The analytical models, (8) and (10), describe the exponential trend; the analytical curve agrees well with the measured points in Fig. 3. The dependence on the temperature is given by the term $\vartheta(T)$ for the mean and $\vartheta^2(T)$ for the variance. Euler's reflection formula yields $\vartheta(T) = a_1\Gamma(1+T/a_2)\Gamma(1-T/a_2)$ with gamma function $\Gamma(\cdot)$ and two coefficients a_1 and a_2. In the region of focus, these functions exponentially increase. The physical understanding of this exponential trend is that the work function of the CNT emitter depends on the temperature. Because the work function W_f is included in the coefficient C_2, the current (1) exponentially changes according to the variation in the work function. In our model, by multiplying the fitting parameter $a(T)$ with C_2, the temperature dependence on the work function is considered. This dependence has been discussed in the literatures, for example, [35], [36], [39]. Notably, it was pointed out in [35] that the fluctuation of the current, which corresponds to the variance $\sigma^2(T)$ in this study, also increases according to the temperature. Our measurement results and the obtained theoretical model describe the same behavior. Therefore, it can be stated that the probability density of the field-emission current is accurately modeled by (7), (8), and (10).

In the signal-processing field, noise variance is a key parameter because it determines important performance metrics, such as the noise power and signal-to-noise ratio. In this field, the influence of the temperature on the power is often evaluated with a noise-temperature model: $k_\mathrm{B}WT$, where W is the bandwidth. The theoretical curve of this model is plotted with a dotted line in Fig. 3(b). Clearly, the slope of the noise-temperature model is quite different from that of the field-emission current. This observation indicates that the existing noise-temperature model is not effective, and our developed noise model should be employed to model field-emission currents in signal-processing systems.

The results obtained here are effective in the wide range of field emitters made of various nanomaterials. Regardless of the material, the behavior of the field emission from a

metal surface is described by the Fowler–Nordheim law. As described in Section II, the temperature dependence can be discussed based on this law. This point has been demonstrated with various emitters, including $W_{18}O_{49}$ nanowires [38], VO_2 nanogap emitters [39], SiC@SiO_2@graphene nanoarray [35] and WS_2 nanosheets [43]. Because our developed model originates from the general model of the Fowler–Nordheim equation, and the obtained exponential trend agrees with the result in the literature, a similar discussion is possible for other types of field emitters. In addition, for the same reason, the derived model should be effective at other applied voltages.

IV. PERFORMANCE ANALYSIS OF NANOMECHANICAL-BASED COMMUNICATION IN TERMS OF TEMPERATURE

Varying the temperature affects systems in which the field-emission current is induced. In this section, we focus on the state-of-the-art nanoscale communication system proposed in [18], and analyze its influence on the quality in the data transmission. In nanoscale communication systems, the field-emission current is the key physical quantity because, as described in Section IV-A, the receiver detects the incoming signal through a nanomechanical device, and the amount of vibration is measured by the current. The influence of the temperature is analytically discussed in Section IV-B by analyzing the BER, a common performance measure in communications systems. The developed noise model (7) is used in the analysis because the BER inherently depends on the probability density of the noise [41]. As predicted, typical performance degradation is found in the numerical results in Section IV-C.

A. BRIEF DESCRIPTION AND ANALYSIS OF NANOMECHANICAL RECEIVER

In the system we are evaluating, a CNT cantilever is installed at the front end of a receiver. The electro-magnetic (EM) waves, which carry the digital data $d_i \in \{+1, -1\}$ with phase modulation, is detected via the mechanical vibration of the CNT tip. When electrons gather at the tip as voltage is applied, Coulomb's law states that an electrostatic force, which is the driving force of the vibration, is excited by the EM wave. The amount of vibration can be observed via the field-emission current. When the vibration amplitude is small relative to the CNT length, the motion of the tip is described by the following second-order linear differential equation,

$$m_{\mathrm{e}}\frac{\mathrm{d}^2x}{\mathrm{d}t^2}+\gamma\frac{\mathrm{d}x}{\mathrm{d}t}+k_0x=Q_{\mathrm{ext}}E_d(t), \tag{11}$$

where m_{e} is the effective mass of the CNT, Q_{ext} is the amount of charge at the tip, and $E_d(t)$ is the EM wave. The coefficients k_0 and γ are given as $k_0=3\pi E_{\mathrm{u}}\rho^4/4L^3$ and $\gamma=2\pi f_{\mathrm{r}}m_{\mathrm{e}}/Q$ with quality factor Q, Young's modulus of CNT E_{u}, and resonance frequency $f_{\mathrm{r}}\equiv(2\pi)^{-1}\sqrt{k_0/m_{\mathrm{e}}}$.

By applying voltage between the CNT tip and the counter electrode (anode), we can observe a field-emission current. Owing to the vibration, the gap length z varies such that $z=z_0+\Delta z(t)$ with the gap variation term $\Delta z(t)$ and length z_0 at the equilibrium point. This variation term leads to changes in the current, which means that the vibration of the CNT tip, which describes the EM wave, can be estimated by observing the variation in the current. The analytical expression of the current with this variation is derived straightforwardly in a manner similar to that in [18],

$$I(t)=\mu_{z_0}(T)+\Delta I(t)+n(t;T), \tag{12}$$

where

$$\Delta I(t)\equiv\chi(T)\mu_{z_0}(T)\cdot x^2(t) \tag{13}$$

$$\begin{aligned}\chi(T)\equiv\frac{1}{2Lb\rho\beta}\Bigg[&\frac{C_2}{E(V)}\left\{v(y)+a(T)-\frac{y\partial_y v(y)}{2}\right\}\\&+\left\{1-\frac{y\partial_y t(y)}{2t(y)}\right\}\\&\cdot\left\{1+\frac{C_3Tt(y)}{E(V)}\tan^{-1}\left(\frac{C_3Tt(y)}{E(V)}\right)\right\}\Bigg],\end{aligned} \tag{14}$$

and $\partial_y\equiv\partial/\partial y$. Clearly, the variation of the current obtained by (13) contains information of the vibration amplitude of the CNT tip. From the discussion in Section III, the current contains noise $n(t;T)$, which follows a Gaussian distribution with zero-mean and the temperature-dependent variance in (10). Note that the mean term $\mu_{z_0}(T)\equiv\mu(T)|_{z=z_0}$ is given by (5).

To estimate the transmitted data from the current, a simple correlator, in which the current is correlated with the sinusoidal signal over the time interval of each data bit T_{b}, is employed at the receiver. Using the resonance frequency f_{r}, the output is obtained as

$$\begin{aligned}r_{f_{\mathrm{r}}}[i]&=\frac{1}{\sqrt{T_{\mathrm{b}}}}\int_{(i-1)T_{\mathrm{b}}}^{iT_{\mathrm{b}}}I(t)\cos\,(2\pi f_{\mathrm{r}}t)\,\mathrm{d}t\\&=-\tilde{\mu}(T)\overline{E}_{\mathrm{ref}}\sqrt{\varepsilon_{\mathrm{b}}}d_i\sin\theta_0+n_i(T),\end{aligned} \tag{15}$$

where ε_{b} is the signal power per data bit, $\overline{E}_{\mathrm{ref}}$ is the bias of the reference field intensity, and θ_0 is the phase difference between the transmitter and receiver [18]. The coefficient

$$\tilde{\mu}(T)\equiv\frac{QQ_{\mathrm{ext}}^2}{k_0^2}\chi(T)\cdot\mu_{z_0}(T) \tag{16}$$

used in (15) describes the influence of the temperature on the signal component, $\sqrt{\varepsilon_{\mathrm{b}}}d_i$. Because $\mu_{z_0}(T)$ increases with increasing temperature, as shown in Fig. 3(a), the signal component may be somewhat amplified. The noise term, $n_i(T)=(1/\sqrt{T_{\mathrm{b}}})\int_{(i-1)T_{\mathrm{b}}}^{iT_{\mathrm{b}}}n(t;T)\cos(2\pi f_{\mathrm{r}}t)\mathrm{d}t$, also depends on the temperature. The characteristic of the noise term is the same as $n(t;T)$ [41]: $n_i(T)$ follows a Gaussian distribution with zero mean and variance (10). The transmitted data $\hat{d}_i$ are then estimated by taking the sign of the statistic, $\hat{d}_i=\mathrm{sgn}(r_{f_{\mathrm{r}}}[i])$.

B. BER ANALYSIS

The BER performance is theoretically analyzed by exploiting the derived model of the noise, (7). The BER is the probability that the estimated data $\hat{d}_i$ do not equal the transmitted data d_i, as follows:

$$\begin{aligned}\mathrm{BER}_{f_\mathrm{r}} &= \Pr[\hat{d}_i \neq d_i] \\ &= \Pr\left[\hat{d}_i = -1 | d_i = +1\right] \Pr[d_i = +1] \\ &\quad + \Pr\left[\hat{d}_i = +1 | d_i = -1\right] \Pr[d_i = -1] \\ &= \frac{1}{2}\Pr\left[r_{f_\mathrm{r}}[i] < 0 | d_i = +1\right] \\ &\quad + \frac{1}{2}\Pr\left[r_{f_\mathrm{r}}[i] > 0 | d_i = -1\right] \\ &= \frac{1}{2}\Pr\left[\xi(T)\overline{E}_\mathrm{ref}\sqrt{\varepsilon_\mathrm{b}}\sin\theta_0 > n_i(T)\right] \\ &\quad + \frac{1}{2}\Pr\left[\xi(T)\overline{E}_\mathrm{ref}\sqrt{\varepsilon_\mathrm{b}}\sin\theta_0 > -n_i(T)\right]. \quad (17)\end{aligned}$$

Note that in the second equality, the data bit d_i is assumed to be equiprobable, and in the third equality, (15) was substituted.

Based on the experimental results, we revealed in (7) that the noise term $n_i(T)$, which should cause an estimation error in the transmitted data, is Gaussian with zero mean and variance $\sigma^2(T)$. This valuable result yields a solvable form of the BER:

$$\begin{aligned}&\Pr\left[\tilde{\mu}(T)\overline{E}_\mathrm{ref}\sqrt{\varepsilon_\mathrm{b}}\sin\theta_0 > n_i(T)\right] \\ &\quad = \frac{1}{\sqrt{2\pi}}\int_{-\infty}^{\tilde{\mu}(T)\overline{E}_\mathrm{ref}\sin\theta_0\sqrt{\varepsilon_\mathrm{b}/\sigma^2(T)}} \exp(-u^2/2)\mathrm{d}u. \quad (18)\end{aligned}$$

Substituting (18) into (17), a simple expression of the BER is obtained:

$$\mathrm{BER}_{f_\mathrm{r}} = \Psi\left(\left|\tilde{\mu}(T)\overline{E}_\mathrm{ref}\sin\theta_0\right|\sqrt{\frac{\varepsilon_\mathrm{b}}{\sigma^2(T)}}\right) = \Psi\left(\sqrt{\zeta(T)}\right), \quad (19)$$

where $\zeta(T) \equiv \overline{E}_\mathrm{ref}^2 \sin^2\theta_0 \varepsilon_\mathrm{b} \tilde{\mu}^2(T)/\sigma^2(T)$ is the effective signal-to-noise power ratio per bit and $\Psi(z) \equiv (1/\sqrt{2\pi}) \cdot \int_z^\infty \exp(-u^2/2)\mathrm{d}u$ is the *Q-function* that represents the tail probability of a standard Gaussian distribution, $\exp(-u^2/2)$.

C. NUMERICAL EXAMPLES OF BER WITH TEMPERATURE

The BER dependence on temperature is discussed in this section through numerical calculation.

The numerical example of BER performance obtained from (19) is plotted in Fig. 4. To calculate the fitting parameters, $a(T)$, b, A, and B, which are involved in $\tilde{\mu}(T)$, we used the experimental data shown in Section III. The parameters $\theta_0 = \pi/2$, $\overline{E}_\mathrm{ref} = 1.0\times10^7$, and $\varepsilon_\mathrm{b} = 3.2\times10^6$ were used, and the values of Q_ext and k_0 were calculated with the method provided in [18].

From Fig. 3, one may expect that increasing temperature has a positive effect on performance because the mean $\mu_{z_0}(T)$, which determines the signal power, as shown in (15) and (16), increases according to temperature. Indeed, because the term $\chi(T)$ is almost constant even with temperature variation, the signal-to-noise power ratio $\zeta(T)$, which determines the BER, varies with the temperature as $\partial\zeta(T)/\partial T \approx \partial\left(\mu_{z_0}^2(T)/\sigma^2(T)\right)/\partial T$. However, as shown in Fig. 4, the BER monotonically increases with increasing temperature. This is because, as observed in Fig. 3, the variance $\sigma^2(T)$ rapidly increases compared to the mean $\mu_{z_0}(T)$, and hence, the signal-to-noise power ratio decreases as the temperature increases. Note that the minimum on the curve, which is observed at 325 K, appears to be due to measurement error and/or the influence of the numerical fitting. To validate this behavior, we calculated the 95% confidence interval of the signal-to-power ratio $\zeta(T)$ at each temperature. The interval was calculated based on the measured data, and provided with error bars in the inset of Fig. 4. All of the points obtained by our derived model are included in the interval. This means that our measurements and the developed model are correct.

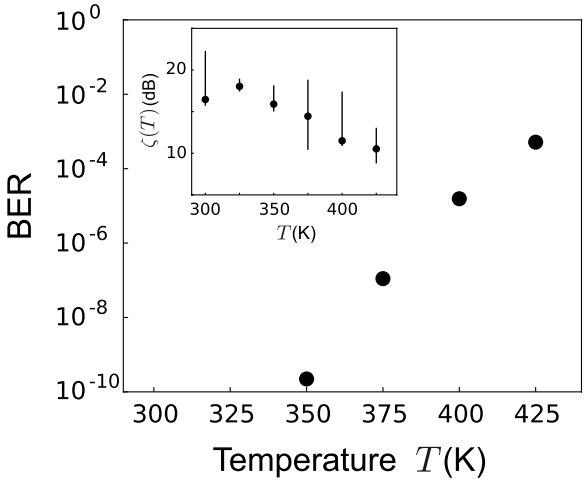

FIGURE 4. BER dependence on temperature. As shown in the inset, the signal-to-noise power ratio, $\zeta(T)$, decreases as the temperature increases, and then the BER increases. To validate the developed model, the 95% confidence interval of the signal-to-power ratio $\zeta(T)$ at each temperature is also provided in the inset. All of the points obtained by the derived model are included in the interval, which means that the developed model is correct.

V. CONCLUSIONS

To support the future development of a wide variety of applications and systems based on field emission, this paper presents a mathematical model of the noise contained in the field-emission current. The model is based on the exploration of the probability density of the noise, and because the current is strongly affected by the temperature, the model is derived in terms of temperature. Our experiment and related analysis reveal that the density follows a Gaussian distribution. An analytic expressions of the two key variables in the distribution, mean and variance, was also derived. The dependence of these variables on the temperature is shown to be exponential, which is noteworthy because in signal processing and communication, temperature is often

considered with a noise-temperature model, namely, linear dependence. Such exponential behavior is likely due to the nonlinear response of the field-emission current. Because the noise model is derived based on the general model of the field emission, it should be effective in other types of the field emitters, including nanowires.

Another contribution of this study is the evaluation of the communication performance of a nanoscale receiver as the temperature varies. This evaluation is made possible by employing our derived model of the probability density. The BER, which characterizes the communication performance, is theoretically discussed and shown to exponentially increase with increasing temperature. From our analysis, the reason was found to be a decrease in the signal-to-noise power ratio. This means that, for the expected future development, the temperature should be kept low such as at room temperature, to secure reliable nanoscale communications.

REFERENCES

[1] J. Robertson, W. I. Milne, K. B. K. Teo, and M. Chhowalla, "Field emission applications of carbon nanotubes," in *Proc. AIP Conf.*, vol. 633, no. 1, 2002, pp. 537–542.

[2] F. G. Rüdenauer, "Field emission devices for space applications," *Surf. Interface Anal.*, vol. 39, nos. 2–3, pp. 116–122, 2007.

[3] I. W. Rangelow, "Sharp silicon tips for AFM and field emission," *Microelectron. Eng.*, vol. 23, no. 1, pp. 369–372, 1994.

[4] J. M. Beebe, B. Kim, J. W. Gadzuk, C. D. Frisbie, and J. G. Kushmerick, "Transition from direct tunneling to field emission in metal-molecule-metal junctions," *Phys. Rev. Lett.*, vol. 97, no. 2, 2006, Art. no. 026801.

[5] N. S. Lee *et al.*, "Application of carbon nanotubes to field emission displays," *Diamond Rel. Mater.*, vol. 10, no. 2, pp. 265–270, 2001.

[6] W. Lei *et al.*, "A graphene-based large area surface-conduction electron emission display," *Carbon*, vol. 56, pp. 255–263, May 2013.

[7] Y. Saito and S. Uemura, "Field emission from carbon nanotubes and its application to electron sources," *Carbon*, vol. 38, no. 2, pp. 169–182, 2000.

[8] S.-M. Lu, W.-Y. Chan, W.-B. Su, W. W. Pai, H.-L. Liu, and C.-S. Chang, "Characterization of external potential for field emission resonances and its applications on nanometer-scale measurements," *New J. Phys.*, vol. 20, no. 4, 2018, Art. no. 043014.

[9] V. B. Neculaes, P. M. Edic, M. Frontera, A. Caiafa, G. Wang, and B. De Man, "Multisource X-ray and CT: Lessons learned and future outlook," *IEEE Access*, vol. 2, pp. 1568–1585, 2014.

[10] S. N. Kazmi *et al.*, "Tunable nanoelectromechanical resonator for logic computations," *Nanoscale*, vol. 9, no. 10, pp. 3449–3457, 2017.

[11] H. Tanaka, T. Ozaki, Y. Ohno, and Y. Tadokoro, "Phase shifter tuned by varying the spring constant of a nanomechanical cantilever," *J. Appl. Phys.*, vol. 122, no. 23, 2017, Art. no. 234501.

[12] P. Hosseini, M. Kumar, and H. Bhaskaran, "2-D materials as a functional platform for phase change tunable NEMS," *IEEE Access*, vol. 3, pp. 737–742, 2015.

[13] I. Mahboob, M. Mounaix, K. Nishiguchi, A. Fujiwara, and H. Yamaguchi, "A multimode electromechanical parametric resonator array," *Sci. Rep.*, vol. 4, p. 4448, Mar. 2014.

[14] A. Yao and T. Hikihara, "Logic-memory device of a mechanical resonator," *Appl. Phys. Lett.*, vol. 105, no. 12, Sep. 2014, Art. no. 123104.

[15] B. Atakan and O. B. Akan, "Carbon nanotube-based nanoscale ad hoc networks," *IEEE Commun. Mag.*, vol. 48, no. 6, pp. 129–135, Jun. 2010.

[16] K. Jensen, J. Weldon, H. Garcia, and A. Zettl, "Nanotube radio," *Nano Lett.*, vol. 7, no. 11, pp. 3508–3511, 2007.

[17] H. Tanaka, Y. Ohno, and Y. Tadokoro, "Angular sensitivity of VHF-band CNT antenna," *IEEE Trans. Nanotechnol.*, vol. 14, no. 6, pp. 1112–1116, Nov. 2015.

[18] Y. Tadokoro, Y. Ohno, and H. Tanaka, "Detection of digitally phase-modulated signals utilizing mechanical vibration of CNT cantilever," *IEEE Trans. Nanotechnol.*, vol. 17, no. 1, pp. 84–92, Jan. 2018.

[19] Y. Tadokoro, H. Tanaka, and M. I. Dykman, "Driven nonlinear nanomechanical resonators as digital signal detectors," *Sci. Rep.*, vol. 8, Jul. 2018, Art. no. 11284.

[20] H. Tanaka, Y. Ohno, and Y. Tadokoro, "Adaptive control of angular sensitivity for VHF-band nano-antenna using CNT mechanical resonator," *IEEE Trans. Mol. Biol. Multi-Scale Commun.*, vol. 3, no. 1, pp. 24–32, Mar. 2017.

[21] Q. H. Abbasi *et al.*, "Nano-communication for biomedical applications: A review on the state-of-the-art from physical layers to novel networking concepts," *IEEE Access*, vol. 4, pp. 3920–3935, 2016.

[22] C. E. Koksal and E. Ekici, "Applications and performance of a nanoreceiver with a carbon nanotube antenna forest," *IEEE Wireless Commun.*, vol. 19, no. 5, pp. 52–57, Oct. 2012.

[23] V. Gouttenoire *et al.*, "Digital and FM demodulation of a doubly clamped single-walled carbon-nanotube oscillator: Towards a nanotube cell phone," *Small*, vol. 6, no. 9, pp. 1060–1065, 2010.

[24] P. Vincent *et al.*, "Performance of field-emitting resonating carbon nanotubes as radio-frequency demodulators," *Phys. Rev. B, Condens. Matter*, vol. 83, no. 15, 2011, Art. no. 155446.

[25] H. G. Craighead, "Nanoelectromechanical systems," *Science*, vol. 290, no. 5496, pp. 1532–1535, 2000.

[26] B. E. DeMartini, J. F. Rhoads, M. A. Zielke, K. G. Owen, S. W. Shaw, and K. L. Turner, "A single input-single output coupled microresonator array for the detection and identification of multiple analytes," *Appl. Phys. Lett.*, vol. 93, no. 5, p. 054102, 2008.

[27] K. Eom, H. S. Park, D. S. Yoon, and T. Kwon, "Nanomechanical resonators and their applications in biological/chemical detection: Nanomechanics principles," *Phys. Rep.*, vol. 503, pp. 115–163, Jun. 2011.

[28] J. Moser *et al.*, "Ultrasensitive force detection with a nanotube mechanical resonator," *Nature Nanotechnol.*, vol. 8, pp. 493–496, Jun. 2013.

[29] V. Puller, B. Lounis, and F. Pistolesi, "Single molecule detection of nanomechanical motion," *Phys. Rev. Lett.*, vol. 110, no. 12, 2013, Art. no. 125501.

[30] S. N. R. Kazmi, A. Z. Hajjaj, M. A. Al Hafiz, P. M. F. J. Costa, and M. I. Younis, "Highly tunable electrostatic nanomechanical resonators," *IEEE Trans. Nanotechnol.*, vol. 17, no. 1, pp. 113–121, Jan. 2018.

[31] E. L. Murphy and R. H. Good, "Thermionic emission, field emission, and the transition region," *Phys. Rev.*, vol. 102, no. 6, pp. 1464–1473, 1956.

[32] P. Hawkes and E. Kasper, *Principles of Electron Optics II: Applied Geometrical Optics*. London, U.K.: Academic, 2017.

[33] M. Lenzlinger and E. H. Snow, "Fowler-Nordheim tunneling into thermally grown SiO_2," *J. Appl. Phys.*, vol. 40, no. 1, pp. 278–283, Nov. 1969.

[34] S. Kolekar, S. P. Patole, S. Patil, J. B. Yoo, and C. V. Dharmadhikari, "Study of thermal-field emission properties and investigation of temperature dependent noise in the field emission current from vertical carbon nanotube emitters," *Surf. Sci.*, vol. 664, pp. 76–81, Oct. 2017.

[35] Z. J. Li *et al.*, "Excellent high temperature field emission behavior with an ultra-low turn-on field and reliable current emission stability from SiC@SiO_2@graphene nanoarray emitters," *J. Mater. Chem. C*, vol. 6, no. 11, pp. 2678–2683, 2018.

[36] Z. Pan *et al.*, "Sensing properties of a novel temperature sensor based on field assisted thermal emission," *Sensors*, vol. 17, no. 3, p. 473, 2017.

[37] P. S. Guo, Z. Sun, S. M. Huang, and Y. Sun, "Temperature effect on field emission properties and microstructures of polymer-based carbon films," *J. Appl. Phys.*, vol. 98, no. 7, 2005, Art. no. 074906.

[38] W. Q. Chen, R. Z. Zhan, S. Z. Deng, N. S. Xu, and J. Chen, "Anomalous temperature dependence of field emission from $W_{18}O_{49}$ nanowires caused by surface states and field penetration ," *J. Appl. Phys.*, vol. 116, no. 13, 2014, Art. no. 133506.

[39] M. Liu, W. Fu, Y. Yang, T. Li, and Y. Wang, "Excellent field emission properties of VO_2(A) nanogap emitters in air," *Appl. Phys. Lett.*, vol. 112, no. 9, 2018, Art. no. 093104.

[40] S. Kay, *Fundamentals of Statistical Signal Processing: Detection Theory*, vol. 2. New Jersey, New York, NY, USA: Prentice-Hall, 1998.

[41] J. G. Proakis, *Digital Communications*. New York, NY, USA: McGraw-Hill, 2001.

[42] M. A. More, R. V. Kashid, S. S. Patil, D. R. Shinde, and D. S. Joag, "Field emission current noise analysis of carbon based materials," in *Proc. 25th Int. Vac. Nanoelectron. Conf.*, 2012, pp. 1–2.

[43] S. R. Suryawanshi, P. S. Kolhe, C. S. Rout, D. J. Late, and M. A. More, "Spectral analysis of the emission current noise exhibited by few layer WS_2 nanosheets emitter," *Ultramicroscopy*, vol. 149, pp. 51–57, Feb. 2015.

[44] N. de Jonge, M. Allioux, J. T. Oostveen, K. B. K. Teo, and W. I. Milne, "Low noise and stable emission from carbon nanotube electron sources," *Appl. Phys. Lett.*, vol. 87, no. 13, 2005, Art. no. 133118.

[45] G. S. Bocharov and A. V. Eletskii, "Theory of carbon nanotube (CNT)-based electron field emitters," *Nanomaterials*, vol. 3, no. 3, pp. 393–442, 2013.
[46] R. H. Fowler and L. Nordheim, "Electron emission in intense electric fields," *Proc. R. Soc. Lond. A, Math. Phys. Sci.*, vol. 119, no. 781, pp. 173–181, May 1928.
[47] R. G. Forbes and J. H. B. Deane, "Reformulation of the standard theory of Fowler–Nordheim tunnelling and cold field electron emission," *Proc. Roy. Soc. A, Math., Phys. Eng. Sci.*, vol. 463, no. 2087, pp. 2907–2927, 2007.
[48] S. M. Sze and K. K. Ng, *Physics of Semiconductor Devices*. Hoboken, NJ, USA: Wiley, 2006.
[49] B. W. Silverman, *Density Estimation for Statistics and Data Analysis*. London, U.K.: Chapman & Hall, 1986.
[50] S. J. Sheather, "Density estimation," *Statist. Sci.*, vol. 19, no. 4, pp. 588–597, 2004.
[51] Y. Tadokoro, "Practical optimal nonlinear filter with estimated noise probability density function," *Nonlinear Theory Appl., IEICE*, vol. 8, no. 1, pp. 58–66, 2017.
[52] M. C. Jones, J. S. Marron, and S. J. Sheather, "A brief survey of bandwidth selection for density estimation," *J. Amer. Statist. Assoc.*, vol. 91, no. 433, pp. 401–407, 1996.
[53] R. Gao, Z. Pan, and Z. L. Wang, "Work function at the tips of multiwalled carbon nanotubes," *Appl. Phys. Lett.*, vol. 78, no. 12, pp. 1757–1759, 2001.

KEITA FUNAYAMA received the B.E. and M.E. degrees in mechanical system engineering from Tohoku University, Miyagi, Japan, in 2013 and 2015, respectively. He is currently pursuing the Ph.D. degree with Nagoya University. He joined Toyota Central Research and Development Laboratories, Inc., Aichi, Japan, in 2015. His current interests include nano-structured mechanical and electronic devices.

HIROYA TANAKA (M'02–SM'17) received the B.E. degree from Saitama University, Saitama, Japan, in 2003, and the M.E. and D.E. degrees from the Tokyo Institute of Technology, Tokyo, Japan, in 2005 and 2008, respectively.

He joined Toyota Central Research and Development Laboratories, Inc., Aichi, Japan, in 2008. His current interests include nano-structured electromagnetic devices, nonlinear circuit elements, and applied radio instrumentation and measurements.

JUN HIROTANI received the Ph.D. degree in engineering from Kyushu University, in 2013.

He is currently an Assistant Professor with the Department of Electronics, Nagoya University. His research interests include nanoscale energy transfer, thermophysical properties of nanomaterials, and flexible electronic devices.

KEIICHI SHIMAOKA received the B.S. degree in mechanical engineering from the Nagoya Institute of Technology, Nagoya, Japan, in 1984.

Since 1979, he has been with Toyota Central Research and Development Laboratories, Inc., Aichi, Japan, where he is currently engaged in the research and development of silicon microsensors and micromachining.

Mr. Shimaoka is a member of the Japan Society for Precision Engineering and the Institute of Electrical Engineers of Japan.

YUTAKA OHNO received the B.E., M.E., and Ph.D. degrees from Nagoya University, in 1995, 1997, and 2000, respectively.

He was a Research Scientist with the Japan Society for the Promotion of Science, in 1999. He became a Research Associate, an Assistant Professor, and an Associate Professor with the Department of Quantum Engineering, Nagoya University, in 2000, 2002, and 2008, respectively, where he became a Professor of the EcoTopia Science Institute, in 2015 and also a Professor of the Institute of Materials and Systems for Sustainability, in 2016. He is currently involved in the explorations of electron transport and optical dynamics in nanocarbon materials, and their applications to novel functional devices.

Dr. Ohno is a member of the Japan Society of Applied Physics, the Physical Society of Japan, the Institute of Electronics, Information and Communication Engineers, the Fullerenes and Nanotubes Research Society, and the American Chemical Society.

YUKIHIRO TADOKORO (M'00–SM'18) received the B.E., M.E., and Ph.D. degrees in information electronics engineering from Nagoya University, Aichi, Japan, in 2000, 2002, and 2005, respectively.

Since 2006, he has been with Toyota Central Research and Development Laboratories., Inc. He was a Research Scholar with the Department of Physics and Astronomy, Michigan State University, East Lansing, MI, USA, in 2011 and 2012, to study nonlinear phenomena for future applications in signal and information processing fields. Since 2019, he has been a Visiting Professor with the Graduate School of Informatics, Nagoya University. His current research interests include nanoscale wireless communication, noise-related phenomena in nonlinear systems, and their applications in vehicles.

Dr. Tadokoro is a Senior Member of the Institute of Electronic, Information and Communication Engineers, Japan.